Applied Catalysis B: Environmental 132–133 (2013) 304–314

Contents lists available at SciVerse ScienceDirect

Applied Catalysis B: Environmental

journal homepage: www.elsevier.com/locate/apcatb

Bismuth vanadate hollow spheres: Bubble template synthesis and enhanced photocatalytic properties for photodegradation

Jingxue Sun, Gang Chen*, Jingzhu Wu, Hongjun Dong, Guihong Xiong

Department of Chemistry, Harbin Institute of Technology, Harbin 150001, PR China

ARTICLE INFO

Article history:
Received 9 August 2012
Received in revised form
16 November 2012
Accepted 2 December 2012
Available online 10 December 2012

Keywords:
Hollow spheres
Bubble template
Photodegradation
Formation mechanism

ABSTRACT

Hollow sphere monoclinic scheelite $BiVO_4$ (*m*-$BiVO_4$) is simply synthesized via a simple hydrothermal method by using urea as guiding surfactant. The forming process is investigated to be the incorporation of bubble guiding, oriented attachment and Ostwald ripening. The heterostructured hollow spheres are built up of truncated octahedrons which are also found to be feasible based on theoretical calculation. The preferred truncated octahedron consists of {0 4 0}, {0 1 1}, and {1 1 0} crystal planes with multiplicities of 2, 2, and 4, respectively. Besides urea, different kinds of organic additives (citric acid, Vitamin C and oleic acid) are also chosen for the synthesis of *m*-$BiVO_4$ to clarify the role of urea. The photocatalytic activities with different morphologies are evaluated on the degradation of Rhodamine B. It is found out that the *m*-$BiVO_4$ with hollow structure shows the optimalizing activity and the reaction rate constant reaches up to 0.035 min^{-1} without adding H_2O_2 as hydroxyl radicals provider. Except for activity, the as-prepared samples have high stability and durability, after four cycling runs of photodegradation of RhB, the photocatalytic ability of as-synthesized *m*-$BiVO_4$ did not show any loss. The degradation of RhB is attributed to intrinsically strong photo-oxidation ability rather than photosensitization and the synthesized samples also shows efficient photocatalytic activity for the degradation of 2-propanol. Meanwhile, the reasons for the superior activity are also carefully investigated.

1. Introduction

It is well known that heterogeneous photocatalysts, an ideal "green" technology, have been widely investigated for the sake of environmental applications [1–5]. Scientific interests in the application of photocatalysts have grown extensively, which mainly involved water splitting and degradation of organic contaminants under UV or visible-light irradiation. Over the past decades, promoting the photocatalytic activities and operating in the frequency range of visible light (or in a wider wavelength region) is the primary target in solar energy conversion [6–10]. Under this consideration, a variety of photocatalysts, such as Ag_3PO_4 [11,12], Bi_3NbO_7 [13], BiOX [14–16], Bi_2WO_6 [17,18], and composites [19–22], have been explored for the sake of overcoming shortcomings of low efficiency or narrow region absorption, since TiO_2 was reported in 1972 [23].

Recently, bismuth vanadate ($BiVO_4$) has attracted researcher' tremendous interest, because of its unique properties, such as ferroelasticity, ionic conductivity, gas sensing, and coloristic properties [24]. Moreover, it is also considered as one kind of excellent photocatalysts, due to its narrow band gap (ca. 2.4 eV) and the outstanding photocatalytic performances on both organic-contaminant degradation and oxygen generation under visible light illumination [24–29]. It is known that $BiVO_4$ mainly exists in three crystalline phases: tetragonal zircon, monoclinic scheelite, and tetragonal scheelite structure [30]. Zhang et al. investigated the photocatalytic performances of $BiVO_4$ with different crystalline phases and found that structure of monoclinic scheelite was superior for the process of photocatalysis [31]. The superior photocatalytic performances were discussed by Wang and co-workers, based on the surface photovoltage (SPV) and transient photovoltage (TPV) techniques [32]. Monoclinic scheelite $BiVO_4$ has been prepared by various methods, such as solid state reaction [33], aqueous process [34], molten salt synthesis [35], hydrothermal process [36], ultrasonic spray pyrolysis [37,38], and chemical bath deposition [39,40].

It is commonly considered that the shape of crystals plays a crucial parameter in the determination of their properties. The architectural control of nano- and micro-crystals with well-defined shapes is an attractive and challenging goal in modern materials chemistry [41]. In recent years, hydrothermal synthesis of monoclinic scheelite $BiVO_4$ is the most accepted method because of its unique superiority in terms of high crystallinity and morphology controlling. Till now, $BiVO_4$ with various morphologies, such as truncated octahedron [26], peanut-shaped [37], spindly microtubes [42], and nanosheets [27], have been successfully

* Corresponding author. Fax: +86 451 86413753.
E-mail address: gchen@hit.edu.cn (G. Chen).

0926-3373/$ – see front matter © 2012 Elsevier B.V. All rights reserved.
http://dx.doi.org/10.1016/j.apcatb.2012.12.002

synthesized via hydrothermal process. Besides, it is reported that micro-/nanohollow structures are of great interest in many current and emerging areas of technology because the void space in hollow particles has been used to modulate refractive index, lower density, increase active area for catalysis, improve the particles' ability to withstand cyclic changes in volume, and to expand the array of imaging markers suitable for early detection of cancer [43]. Till now, only a few reports are focused on the synthesis of $BiVO_4$ with hollow structure [44,45], and to the best of our knowledge, there is no report about the simple hydrothermal synthesis of hollow $BiVO_4$ constructed by truncated octahedrons. From another point of view, during the hydrothermal process, organic additives are always adopted, such as PVP, EDTA, and SDBS. It is known that most of the organic additives are costly and hard to remove. Thus, it is an attractive challenge to develop a way of synthesizing monoclinic scheelite $BiVO_4$ with specific morphology, hollow sphere for example, via hydrothermal process by using cost-effective and easily removed organic additives.

In our work, hollow sphere monoclinic scheelite $BiVO_4$ is simply synthesized via a simple hydrothermal method by using urea as guiding surfactant. The choosing of urea is based on the following considerations. Urea is cost effective for commercial applications and water soluble for removing. Besides, urea will decompose to NH_3 which can be used as bubble template for synthesizing hollow structure. The physicochemical properties and formation mechanism of the as-prepared powders have been investigated in detail. The photocatalytic performances are evaluated by degrading rhodamine B (RhB) and 2-propanol as representative, under visible light irradiation ($\lambda > 400$ nm).

2. Experimental

2.1. Catalysts preparation

The monoclinic scheelite $BiVO_4$ powders were prepared using a simple hydrothermal method. All materials were purchased from commercial sources (analytical grade) and used without further purified. In a typical synthesis, 0.0015 mol bismuth nitrate ($Bi(NO_3)_3{\cdot}5H_2O$), 0.0015 mol ammonium metavanadate (NH_4VO_3) and 0.1 g urea ($CO(NH_2)_2$) were dissolved in 30 mL deionized water under vigorous magnetic stirring, and then the pH of the resulting solution was adjusted to 1 with HNO_3 (65–68 wt%) solution. After stirring for 1 h, the suspension was transferred into a 40 mL Teflon-lined stainless steel autoclave to perform hydrothermal process at 180 °C for 12 h. After cooled down to room temperature, the solid product was collected by centrifugation (2000 rpm) and washed with deionized water for five times. The target monoclinic scheelite $BiVO_4$ was finally obtained by drying at 60 °C for 12 h. Besides, other samples were also prepared under identical conditions by changing pH, surfactant, hydrothermal temperature and hydrothermal time.

2.2. Characterization

The structure of the obtained monoclinic scheelite $BiVO_4$ was confirmed by X-ray diffraction (XRD) on Rigaku D/max-2000 diffractometer with Cu Kα radiation ($\lambda = 0.15406$ nm). Diffraction patterns were collected from 10° to 90° at a speed of 4°/min with a scan width of 0.02°. The morphology of the products was observed by a Camscan MX2600FE field emission scanning electron microscope (FE-SEM). The operating voltage was set to 20 kV and the sample was prepared by dropping the pre-ultrasonic-dispersed (10 min) ethanol turbid liquid onto the chip of silicon. Transmission electron microscopy (TEM) and high-resolution TEM (HR-TEM) of the hierarchical structures were carried out on FEI Tecnai G2 S-Twin operating at 300 kV. UV–vis diffuse reflectance spectra were acquired by a spectrophotometer (TU-1900) and $BaSO_4$ was used as the reflectance standard.

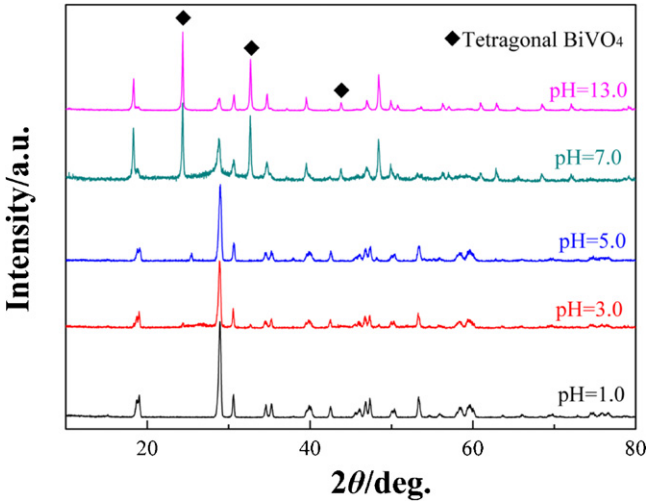

Fig. 1. XRD patterns of $BiVO_4$ synthesized under different value of pH.

2.3. Photocatalytic reactions

Rhodamine B (RhB), one of the biodegradation resistant N-containing dyes, is a popular probe molecule in the heterogeneous photocatalysis reaction. The photocatalytic activities were determined by the degradation of RhB aqueous solution under visible light irradiation ($\lambda > 400$ nm) in quartz photochemical reactor. A 300 W Xenon lamp (Trusttech PLS-SXE 300, Beijing) covered with a UV filter was used as a light source. The process of photodegradation was carried out at ambient temperature as follows: 0.0100 g of photocatalyst was added into 100 mL RhB, sonicated for 15 min and kept in dark for 1 h to reach adsorption–desorption equilibrium under magnetically stirring before irradiation. At given time intervals (10 min), 3 mL mixture was colleted out from the suspension, followed by centrifuged at 10,000 rpm for 5 min. The concentration of RhB was analyzed by measuring the absorbance at $\lambda = 553$ nm. For photodegradation of 2-propanol, 100 mg photocatalyst was transferred into a quartz cell with an aqueous solution of 2-propanol (2.6 μmol dm^{-3}, 15 mL). Prior to irradiation, the suspension was stirred for 1.5 h in dark. The sample was then irradiated with visible light with continuous stirring under O_2 atmosphere in the system. During the photoreaction, the product is analyzed by gas chromatography and mass spectrometry.

3. Results and discussion

3.1. Structure characterization

It is well known that the initial pH value of the precursor solution plays an important role in the formation of the monoclinic scheelite $BiVO_4$ microstructures. Therefore, different samples were prepared under different values of pH. The XRD patterns of the as-synthesized products illustrate that low value of pH is contributes to the formation of monoclinic scheelite $BiVO_4$ (*m*-$BiVO_4$) while high value of pH promotes the generation of tetragonal structure (*t*-BiVO4), as shown in Fig. 1. On account of the superior photocatalytic activity of *m*-$BiVO_4$, the synthesizing processes were carried out under a pH value of 1.0. Fig. 2 shows a typical XRD pattern of synthesized $BiVO_4$ by using urea as a template, which clearly indicates that the sample is made up entirely of *m*-$BiVO_4$. Based on the powder XRD data, the lattice parameters were determined as $a = 5.1896$ Å, $b = 11.7107$ Å, $c = 5.1016$ Å, and $\beta = 90.41°$, which are

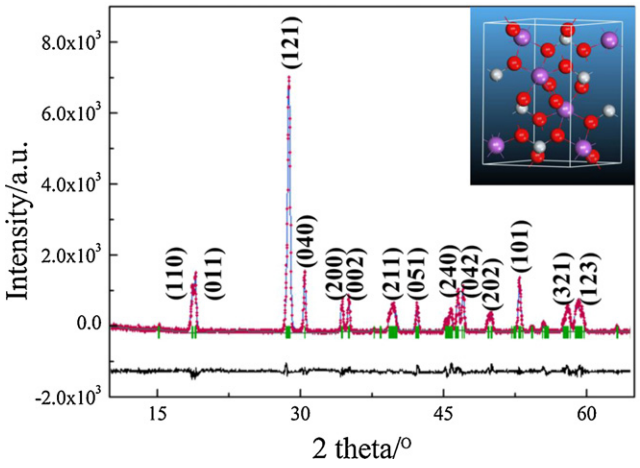

Fig. 2. XRD and Rietveld refinement pattern (crystal model insert) of *m*-$BiVO_4$.

similar with that from the literature (JCPDS card No. 14-0688). Rietveld refinement fitting results are also depicted in Fig. 2. The experimental intensity data are shown by a dotted line, while the solid line represents the calculated pattern. The bottom line corresponds to the difference between the observed and calculated pattern. The vertical bars denote the Bragg positions of *m*-$BiVO_4$. The reliability factors R_{wp} and R_p are refined as 0.0913 and 0.0611, respectively.

3.2. Morphology and forming mechanism

The morphologies of the as-prepared *m*-$BiVO_4$ assisted by urea were further investigated by FE-SEM and TEM. The FE-SEM image (Fig. 3a) shows that the as-prepared *m*-$BiVO_4$ is well-defined hollow sphere with a diameter ca. 4–5 μm. Further observation demonstrated that the hollow sphere is composed of truncated octahedron with a size of about 0.5–1 μm. It is suggested that the hollow structure of *m*-$BiVO_4$ is produced by the bubbles generated from the decomposing of urea. For further investigation of the formation of the truncated octahedron, the theoretical morphology of the *m*-$BiVO_4$ is calculated and depicted in Fig. 3d. As shown, the preferred truncated octahedron consists of {0 4 0}, {0 1 1}, and {1 1 0} crystal planes with multiplicities of 2, 2, and 4, respectively. The total facet area of {0 4 0}, {0 1 1}, and {1 1 0} crystal planes are 25%, 37.5%, and 37.5%, respectively. The corresponding TEM image demonstrates that the *m*-$BiVO_4$ shows morphology of sphere and the HRTEM image is also shown. As can be seen in the HRTEM image (Fig. 3c), the *d*-spacings measured from the reduce FFT are 2.61 and 2.54 Å, which well agree with the lattice spacings of (2 0 0) and (0 0 2) *m*-$BiVO_4$, indicates that the growth direction is along the *c* axis. Thus the (0 4 0) facet is exposed by the formation of truncated octahedron, which is beneficial for the improving of

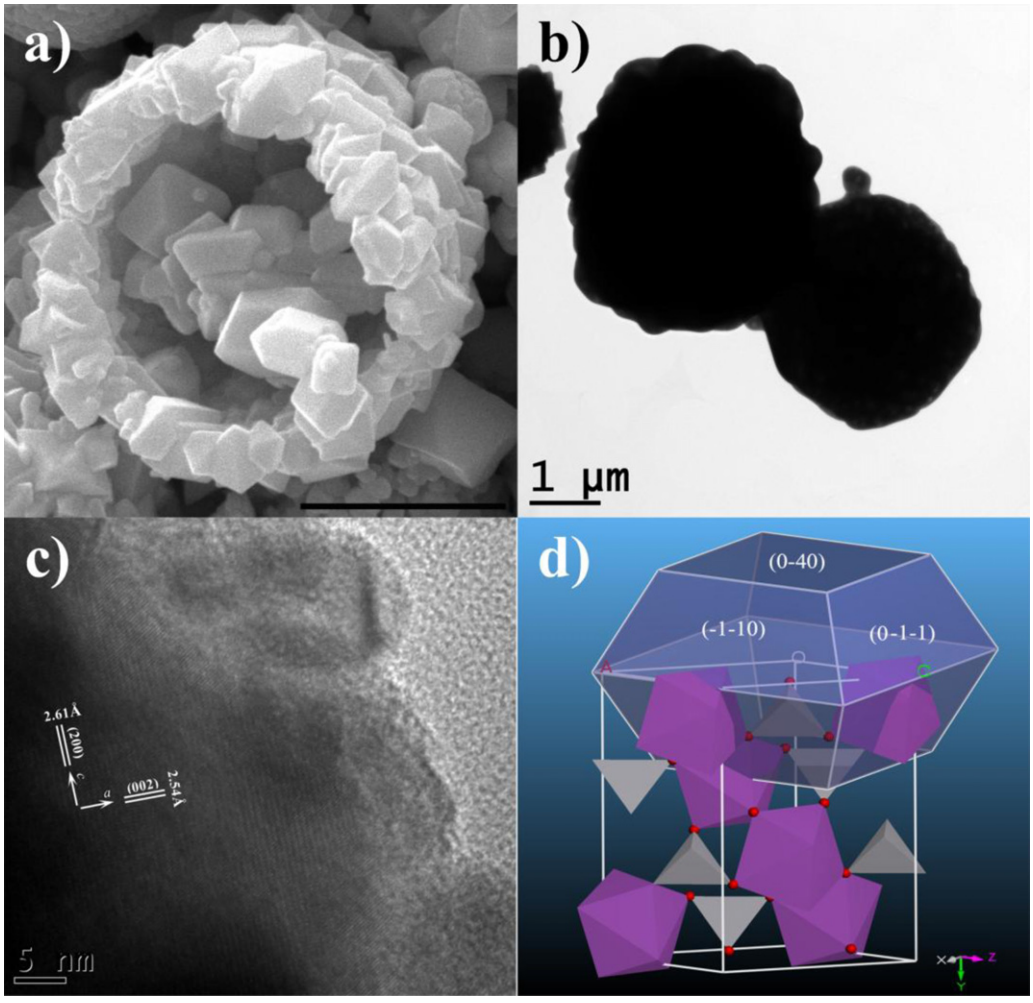

Fig. 3. (a) SEM image (scale bar = 2 μm), (b) TEM image, (c) HRTEM images of hollow *m*-$BiVO_4$, and (d) morphology simulation of *m*-$BiVO_4$.

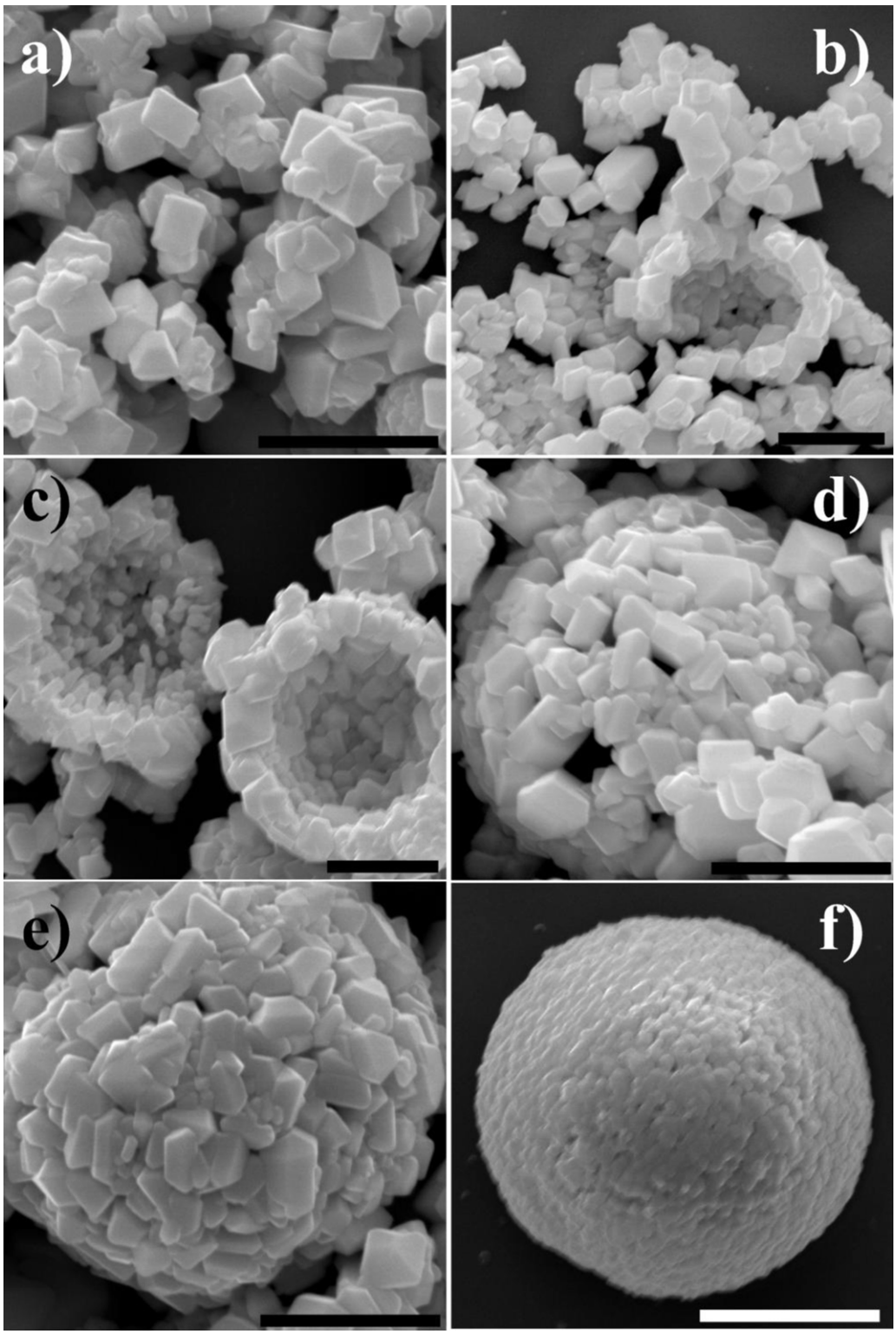

Fig. 4. Morphology evolution of *m*-$BiVO_4$ (a) 2 h, (b) 4 h, (c) 6 h, (d) 8 h (e) 12 h, and (f) 24 h. The scale bar is 2 μm.

the photocatalytic activities, because the active sites with a BiV_4 structure is exposed on the (0 4 0) facet [26].

To investigate the formation process of hollow sphere *m*-$BiVO_4$, a detailed time course experiment is carried out. Fig. 4 shows the representative SEM images of different shaped *m*-$BiVO_4$ during the assembling and ripening procedure. At the initial stage, the product shows morphology of truncated octahedron, and the crystal structure at this stage is confirmed to be pure *m*-$BiVO_4$, see Fig. 5. This sort of truncated octahedron is considered to be the primary structure of the hollow sphere. During this process, the major chemical reactions in the aqueous solution could be formulated as follows [46,47]:

$$NH_2CONH_2 + H_2O \rightarrow 2NH_3 + CO_2 \quad (1)$$

$$Bi(NO_3)_3 + H_2O \rightarrow BiONO_3 + H^+ + 2NO_3^- \quad (2)$$

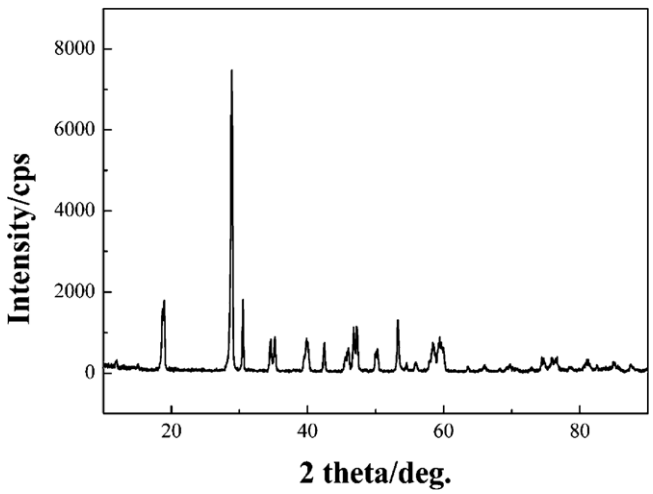

Fig. 5. XRD pattern of the truncated octahedron structured $BiVO_4$.

$$BiONO_3 + VO_3^- \rightarrow BiVO_4 + NO_3^- \quad (3)$$

Thus it can be seen, urea plays a crucial role in the formation of hollow *m*-$BiVO_4$. During the hydrothermal process, urea hydrolyzes in the aqueous solution to produce NH_3 and CO_2 gas, which exist in the form of bubbles. These bubbles can be employed as soft templates, around which the existing truncated octahedrons can aggregate and further grow. As shown in Fig. 4b–d, the truncated octahedron aggregate around the surface of bubbles and then the hemisphere, loose-packed hollow sphere and tight-packed hollow sphere are observed successively. The second step involves the Ostwald ripening process which causes the coarsening and recrystallization of the truncated octahedron crystallites encapsulating the gas bubble [48]. During the process of ripening, shape edges and corners of the truncated octahedrons trend to dissolve, and the supersaturated concentration courses the recrystallization of *m*-$BiVO_4$ at the valleys and cavities of the sphere. The tight-hollow sphere is finally formatted after a ripening process of 24 h. As described in Scheme 1, the morphology evolution mainly involves four steps. First, the *m*-$BiVO_4$ is crystallized under the hydrothermal condition and the truncated octahedrons are generated based on the crystal nucleus. Meanwhile, urea decomposes into gas, and the gas bubbles are then formed around the crystallized *m*-$BiVO_4$. Secondly, hollow hemispheres are formed by the aggregation of truncated octahedron around the gas bubbles. Finally, the hemispheres evolve to sphere, followed by a process of Ostwald ripening into tight-packed hollow spheres.

For comparison, besides urea, different kinds of organic additives (citric acid, Vitamin C and oleic acid) are also chosen for the synthesis of *m*-$BiVO_4$ to clarify the role of urea. It is noted that samples with different morphologies are obtained only by adjusting the selected surfactant. SEM images obtained under different conditions are shown in Fig. 6. As shown, tight spheres are observed when citric acid and Vitamin C are used as additives. Nevertheless, differences can be indicated on the basis of SEM observation. For citric acid, the spheres are composed of truncated octahedrons while some of the truncated octahedrons show a trend to ripening. The size of the sphere is characterized to be 10–20 μm (Fig. 6a and b). For the addition of Vitamin C as surfactant, no truncated octahedrons are observed on the surface of the spheres. The tight spheres are composed of random particles and the size of the spheres are 6–8 μm, as shown in Fig. 6c and d. Unlike the morphology of tight spheres obtained under the assistant of citric acid and Vitamin C, the as-synthesized *m*-$BiVO_4$ in the presence of

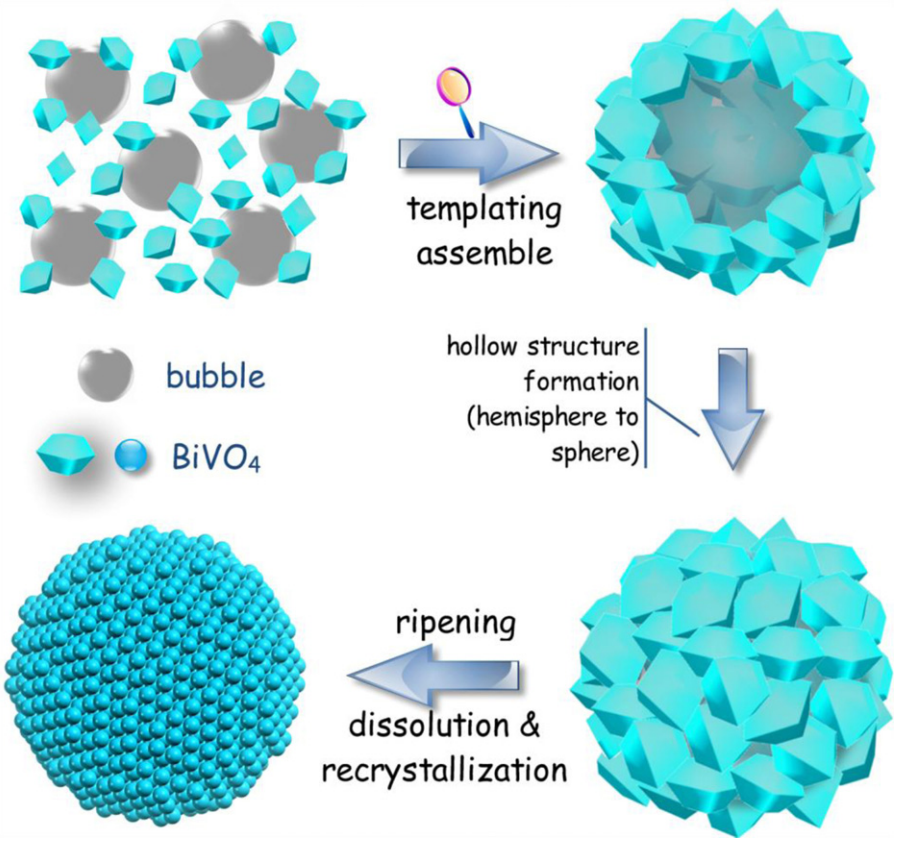

Scheme 1. Sketch map of the evolution of morphology changing of *m*-$BiVO_4$.

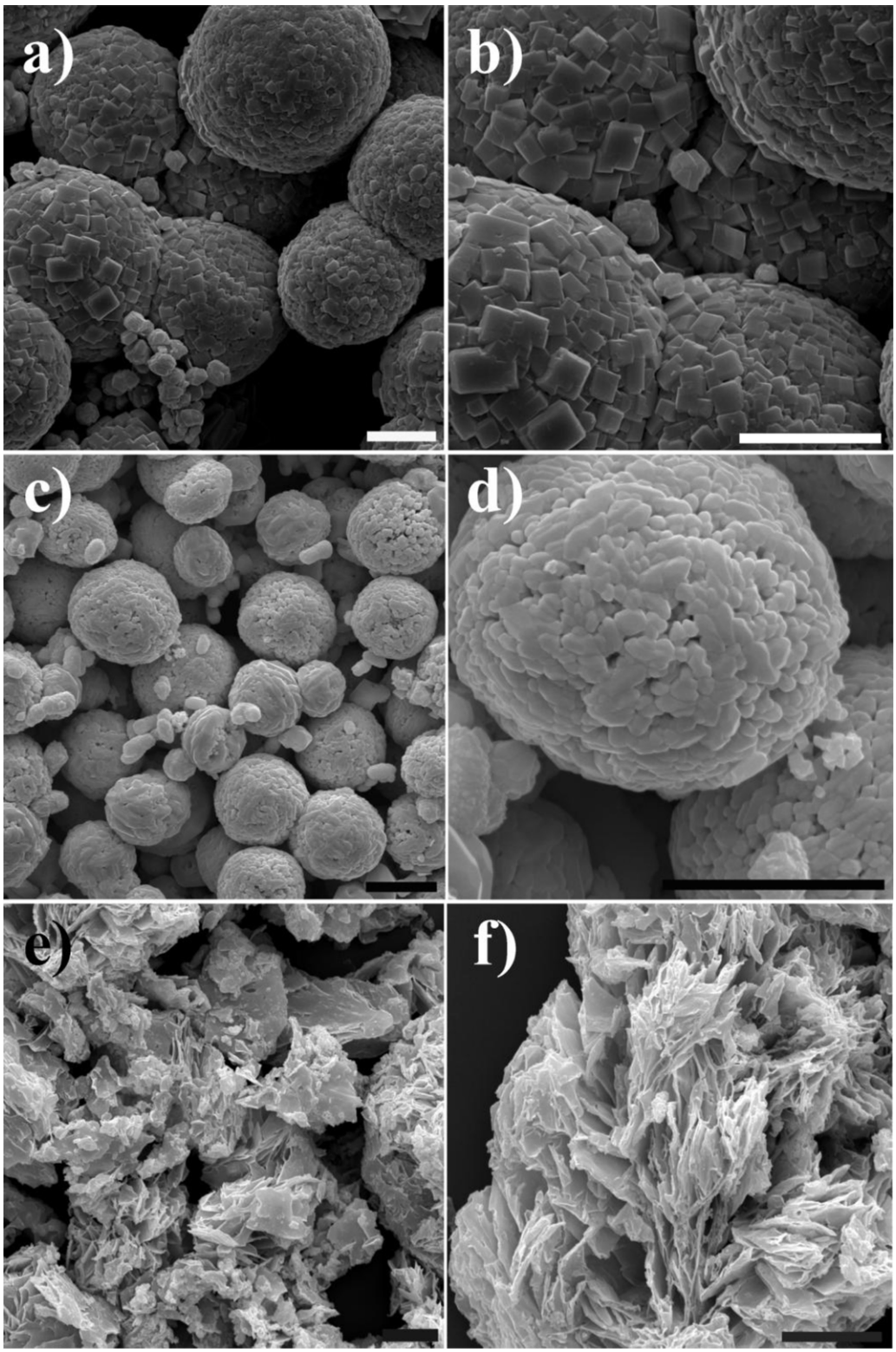

Fig. 6. $BiVO_4$ samples synthesized with different organic additives: (a and b) citric acid, (c and d) Vitamin C, (e and f) oleic acid. The scale bar is 5 μm.

oleic acid is composed of nanosheets with a size of 10–20 μm and thickness of 30–80 nm.

3.3. Light absorbance

Illustrated in Fig. 7 are the UV–vis DRS spectra of the as-fabricated samples under the assistance of different organic additives. It is considered that all the samples exhibit strong visible light absorption except for that of using oleic acid as surfactant. The steep absorption edge in the visible-light region of *m*-$BiVO_4$ samples reveals that the visible-light absorption is due to the bandgap transition [49]. The difference of the as-synthesized *m*-$BiVO_4$ is due to the remnants of organic additives on the surface of the powder.

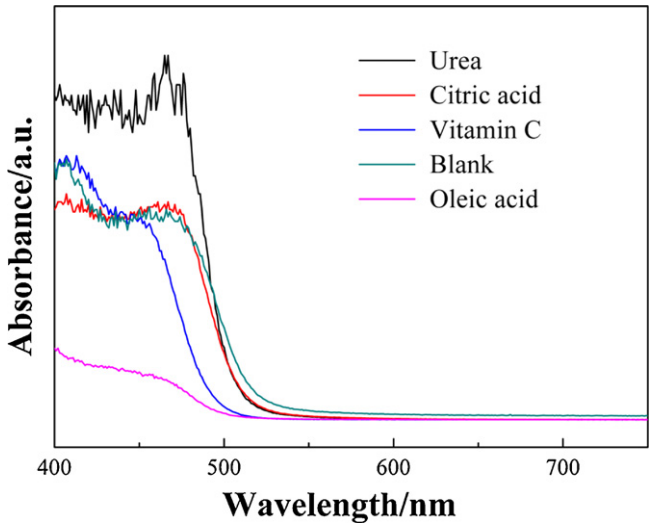

Fig. 7. UV–vis absorbance spectra of $BiVO_4$ samples synthesized with different organic additives.

The band gaps of the as-fabricated samples under the assistance of different additives are also investigated, as shown in Fig. 8. Their band gaps could be determined with the formula $\alpha h\nu = A(h\nu - E_g)^{n/2}$, where α, h, ν, A, E_g, and n are the absorption coefficient, Planck's constant, the incident light frequency, constant, the band-gap energy, and an integer, respectively. Among them, n depends on the characteristics of the optical transition of the semiconductor, $n = 1$ for direct transition semiconductors and $n = 4$ for indirect transition semiconductors. m-$BiVO_4$ is a typical kind of direct transition semiconductors and the values of n are chosen to be 1 [25,24,50]. The corresponding band-gap energy (E_g value) of m-$BiVO_4$ can be thus estimated from a plot of $(\alpha h\nu)^2$ versus the photon energy ($h\nu$). As described in Fig. 6, the band gap energies of different samples synthesized under the assistant of urea, citric acid, Vitamin C and oleic acid. The band gap ranges from 2.5 to 3.3 eV, which is comparable to those of monoclinic $BiVO_4$ reported. The large band gap of the as-synthesized $BiVO_4$ assisted by oleic acid is because of the blue shift caused by the nanometer-sized effect of the nanosheets. The conduction band edge (E_{CB}) and valence band edge (E_{VB}) are key factors that should be investigated [51]. The conduction band edge of a semiconductor at the point of zero charge (pH_{zpc}) can be theoretically predicted from the formula:

$$E^0_{CB} = X - E_c - 0.5E_g$$

where X is the absolute electronegativity of the semiconductor, E_c is the energy of free electrons on the hydrogen scale (4.5 eV). For m-$BiVO_4$, the value of X is 6.035 [41,51]. According to the values of E_g estimated above and the foregoing formula, the calculated E_{CB} and E_{VB} of m-$BiVO_4$ assisted by urea are 0.29 eV and 2.79 eV, respectively. For other organic additives, the calculated E_{CB} and E_{VB} of m-$BiVO_4$ are 0.25 eV and 2.74 eV for citric acid, 0.10 eV and 2.98 eV for Vitamin C, −0.12 eV and 3.18 eV for oleic acid, respectively. For comparison, the E_{CB} and E_{VB} of m-$BiVO_4$ without adding any surfactant are 0.29 eV and 2.78 eV.

3.4. Photocatalytic performance and photocatalytic mechanism

The photocatalytic activities of the m-$BiVO_4$ assisted by different additives are evaluated on the degradation of Rhodamine B. As shown in Fig. 9, the hollow sphere of m-$BiVO_4$ assisted by urea shows the highest activity in degrading RhB compared to the other samples. The removal rate is more than 80% even without adding any H_2O_2 after 50 min reaction of irradiation. Except for urea, Vitamin C and citric acid are both beneficial for the improving of photocatalytic activity. Conversely, the adding of oleic acid restrained the degradation rate of RhB, which is proposed due to the disadvantage of light absorbance. In order to investigated the

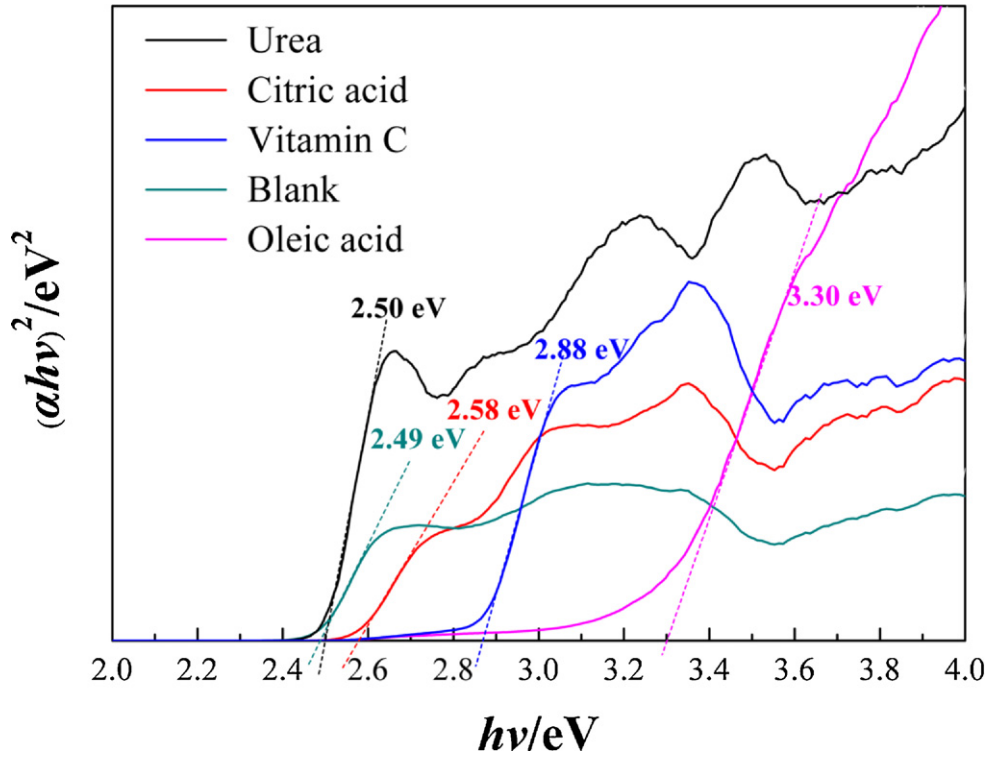

Fig. 8. Calculated band gap of $BiVO_4$ samples synthesized with different organic additives with plots of $(\alpha h\nu)^2$ versus the photon energy ($h\nu$).

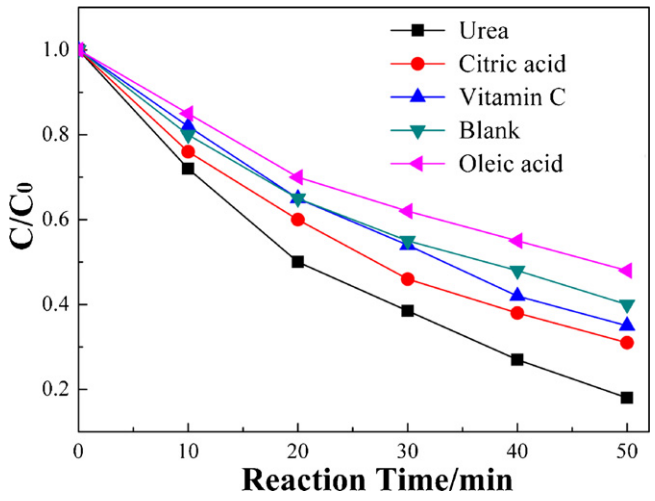

Fig. 9. Photodegradation of RhB dye with $BiVO_4$ samples synthesized with different organic additives.

photoreaction model of the *m*-$BiVO_4$ series, the relation between $\ln(C_0/C)$ and irradiation time (t) is plotted in Fig. 10. As shown in Fig. 8, the linear dependence is clearly observed for the decolorization of RhB solution by the *m*-$BiVO_4$ series synthesized assisted by different organic additives. This means that the photoreactions follow the first-order reaction kinetics, corresponding to the kinetics formula:

$$\ln\left(\frac{C_0}{C}\right) = kt$$

where k is the reaction rate constant. The reaction rate constant of *m*-$BiVO_4$ photocatalysts assisted by urea, citric acid, Vitamin C, none and oleic acid are 0.035 min^{-1}, 0.023 min^{-1}, 0.022 min^{-1}, 0.018 min^{-1}, and 0.014 min^{-1}, respectively. The corresponding correlation coefficients R^2 are 0.999, 0.995, 0.999, 0.998, and 0.998, respectively. The excellent fitness indicates that the photoreaction follows the way of first-order reaction kinetics. Fig. 11 shows the time-evolution of the spectral changes of the RhB mediated by *m*-$BiVO_4$ synthesized assisted by urea. It can be seen obviously that the deep pink color of the starting RhB solution almost fades completely only with the exposure time increasing to 50 min. Meanwhile, the main absorption peak of RhB weakens along with the irradiation

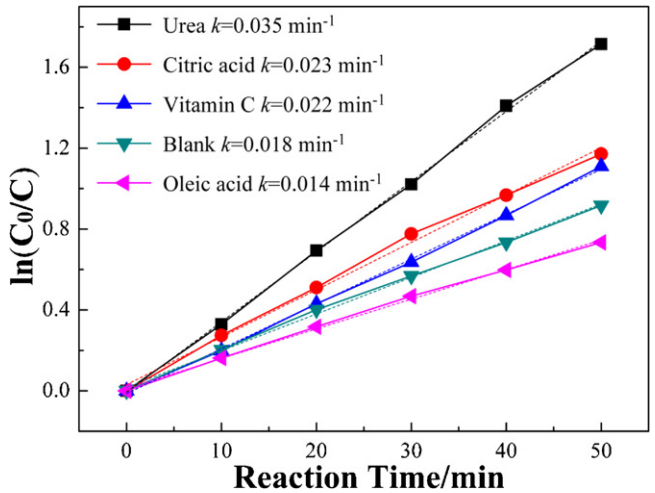

Fig. 10. Calculation of the reaction rate constants of $BiVO_4$ samples synthesized with different organic additives.

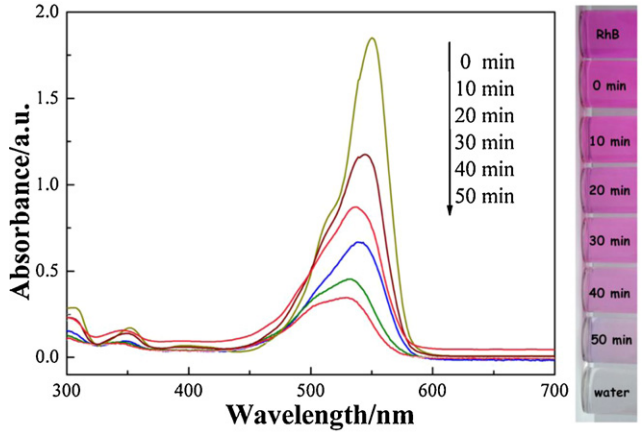

Fig. 11. UV–vis spectral changes of RhB as a function of irradiation time over *m*-$BiVO_4$ hollow sphere.

and no new absorption bands are found in both the ultraviolet and visible regions.

The superior activity of *m*-$BiVO_4$ synthesized with urea is supposed to attribute to the following reasons: First, the Brunauer Emmett Teller (BET) surface area of the hierarchical hollow sphere is estimated to be about 10.6 $m^2\,g^{-1}$, which was much higher than that of the tight sphere composed of octahedron synthesized without any surfactant (3.3 $m^2\,g^{-1}$), as shown in Fig. 12. The high surface area and plenty of pores in this hierarchical structure bring not only more surface reached by the visible light but also more active catalytic sites, which results in good photocatalytic performance. Second, the large hollow space inside the microspheres greatly decreases the density of *m*-$BiVO_4$, so they can be easily suspended in the water. Last but not least, the (0 4 0) facet is exposed by the formation of truncated octahedron, which is beneficial for the improving of the photocatalytic activities, because the active sites with a BiV_4 structure is exposed on the (0 4 0) facet. Furthermore, the remarkable photocatalytic activity has nothing to do with the urea during the photoreaction because no urea is remained on the surface of *m*-$BiVO_4$ which is confirmed by FT-IR. As shown in Fig. 13, compared to the spectra of pure urea, no characteristic peaks of urea is observed on the sample of the

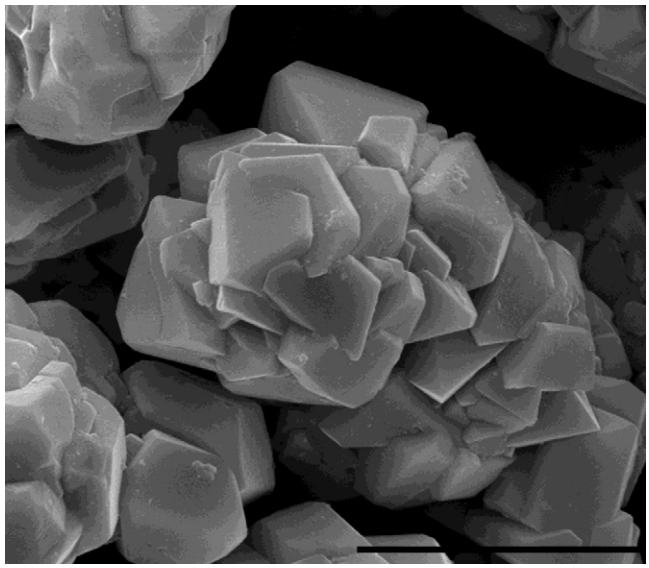

Fig. 12. SEM image of $BiVO_4$ synthesized without any surfactant, the scale bar is 5 μm.

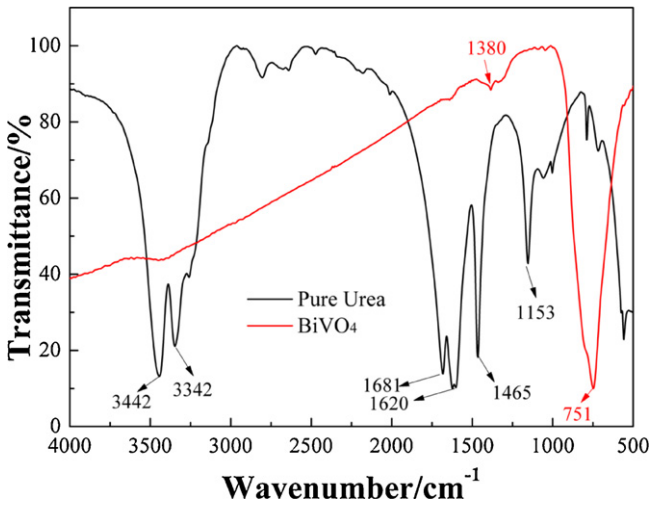

Fig. 13. FT-IR spectra of the synthesized $BiVO_4$ and pure urea.

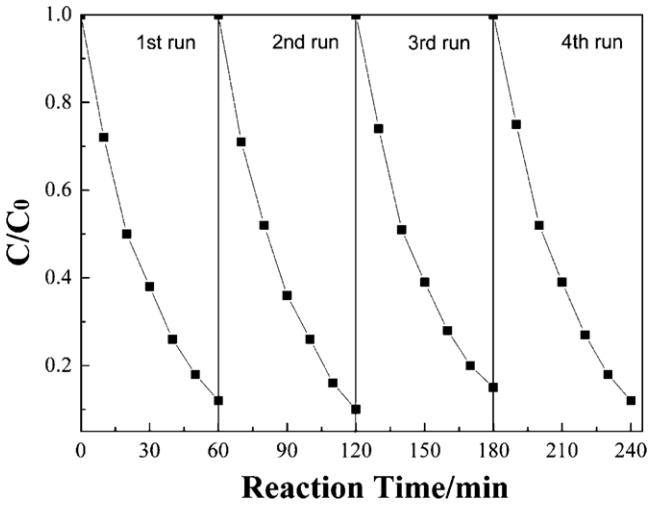

Fig. 15. Decrease of RhB concentration during the recycled experiments over *m*-$BiVO_4$ hollow sphere.

as-synthesized *m*-$BiVO_4$. The spectrum of precursor demonstrates a strong absorption at 751 cm^{-1} can be attributed to the vibration absorption of ν_1 (VO_4) and ν_3 (VO_4) and the band at 1380 cm^{-1} may be assigned to the absorbed CO_2 in the air [42].

To further make the reaction mechanism clear, the effects of capping additives are examined during the photodegradation processes. It is reported that benzoquinone (BQ), ethylenediaminetetraacetic acid (EDTA) and tertiary butanol (TBA) are typical trapping reagents for $O^{2-\bullet}$, holes and $OH^{\bullet}$, respectively [52,53]. As shown in Fig. 14, EDTA leads to are markable inhibiting effect to photodegradation while BQ and TBA have little to do with the photoreaction. The results confirm that photo-generate holes play the most important role in the mineralization of RhB. It is supposed that in *m*-$BiVO_4$ $O^{2-\bullet}$ radicals are almost nonexistent, because the CB edge of *m*-$BiVO_4$ is located at ca. 0.29 V versus normal hydrogen electrode (NHE, pH = 0); thus, its photogenerated electrons cannot easily be captured by O_2 to form $O^{2-\bullet}$. Meanwhile, the standard redox potential of Bi^{5+}/Bi^{3+} is more negative than that of $OH^{\bullet}/OH^{-}$ (+1.99 V), because the standard redox potential of Bi_2O_4/BiO^{+} (Bi^{5+}/Bi^{3+}) (E = 1.59 V at pH = 0) can be a rough estimate of the oxidation potential of the hole (Bi^{5+}) photogenerated in the *m*-$BiVO_4$ photocatalyst [37]. So, the holes photogenerated on the surface of *m*-$BiVO_4$ could hardly react with OH^{-}/H_2O to form $OH^{\bullet}$ radicals.

In consideration of practical applications, the reuse and stability properties are also the important evaluation criterions of the photocatalysts. The recycled experiments are carried out under simulated sunlight irradiation to evaluate the photostability of the hollow *m*-$BiVO_4$ synthesized with urea. After every 60 min photoreaction, the photocatalyst is separated out of the solution by centrifugation and then washed back into the reactor with distilled water in order to keep the initial concentration of RhB and photocatalysts constant. The concentration of the RhB solution during every cycle is shown in Fig. 15. As can be seen, after four cycling runs of photodegradation of RhB, the photocatalytic ability of as-synthesized *m*-$BiVO_4$ did not show any loss, indicating that the as-prepared samples have high stability and durability.

In order to investigate the photodegradation mechanism of dyes, experiment was applied to identify photodegradation patterns including self-oxidation of semiconductor and/or effects of photosensitization. It is found that the main absorption range of RhB is 500–600 nm, as shown in Fig. 11. Meanwhile, $BiVO_4$ synthesized with urea can be only excited by irradiation that the wavelength is shorter than 496 nm (corresponding to 2.5 eV), see Fig. 8. Therefore, monochromatic light with a wavelength of 550 nm (±15 nm) is used to excite RhB molecules rather than $BiVO_4$. As shown in Fig. 16, the result shows that after 60 min irradiation,

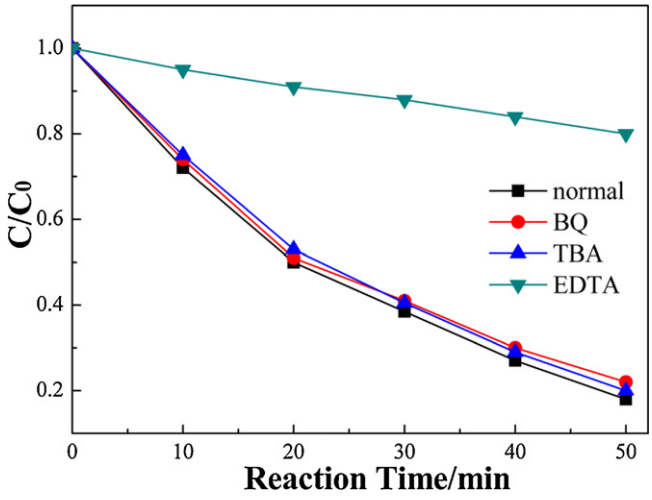

Fig. 14. The effects of various additives on decomposing RhB.

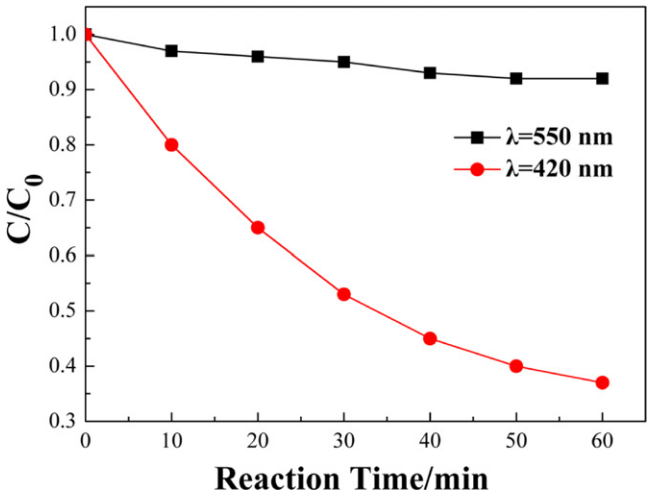

Fig. 16. Photocatalytic properties of $BiVO_4$ under different monochromatic light.

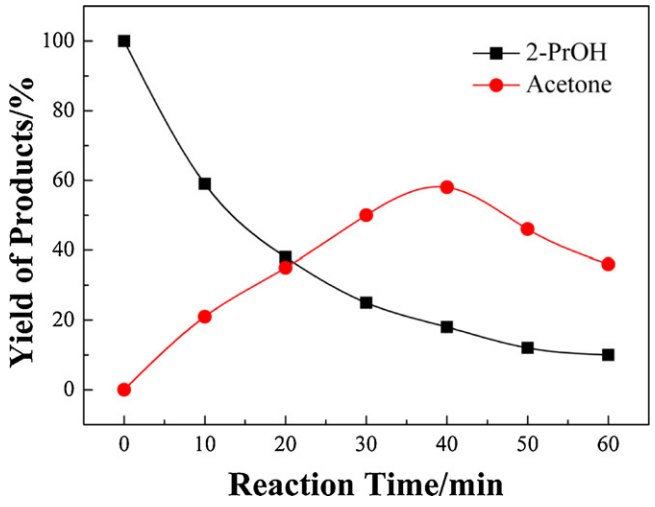

Fig. 17. Photocatalytic degradation of 2-PrOH on $BiVO_4$ photocatalyst.

only less than 8% of RhB is decomposed. It is thus illustrates that the effect of photosensitization is negligible. In contrast, when 420 nm monochromatic light is used, at where only $BiVO_4$ can be excited, photodegradation progress can be clearly observed. Hence, it is suggested that degradation of RhB is attributed to intrinsically strong photo-oxidation ability rather than photosensitization.

Meanwhile, it has been suggested by several authors that the use of organic dyes as a test compound for photocatalytic activity is inadequate [54–57]. In order to further investigate the photocatalytic activity of synthesized $BiVO_4$ with the addition of urea, 2-propanol is selected as substrate which do not absorb in visible region. Prior to irradiation, the suspension was stirred for 1.5 h in dark. The sample was then irradiated with visible light with continuous stirring under O_2 atmosphere in the system. During the photoreaction, the product is analyzed by gas chromatography and mass spectrometry. As can be seen in Fig. 17, it is found that 2-propanol can be steadily oxidized into acetone. After 1 h irradiation, more than 80% 2-propanol can be oxidized. Meanwhile, the amount of acetone increases firstly and then decreases at different reaction time, indicating that along with the time prolonged the acetone can be further decomposed into CO_2 and H_2O.

4. Conclusions

In summary, we have successfully synthesized hollow sphere *m*-$BiVO_4$ via a simple hydrothermal method by using urea as guiding surfactant. The morphology evolution involves nucleation, bubble guiding attachment and Ostwald ripening. The heterostructure hollow spheres are built up of truncated octahedrons consisting of {0 4 0}, {0 1 1}, and {1 1 0} crystal planes with multiplicities of 2, 2, and 4, respectively. Besides urea, different kinds of organic additives (citric acid, Vitamin C and oleic acid) are also chosen for the synthesis of *m*-$BiVO_4$ and different morphologies are directly obtained. It is found out that the *m*-$BiVO_4$ with hollow structure shows the optimalizing activity and the reaction rate constant reaches up to 0.035 min^{-1}. After four cycling runs of photodegradation of RhB, the photocatalytic ability of as-synthesized *m*-$BiVO_4$ did not show any loss, indicating that the as-prepared samples have high stability and durability. Furthermore, the degradation of RhB is attributed to intrinsically strong photo-oxidation ability rather than photosensitization and the synthesized sample shows efficient photocatalytic activity for the degradation of 2-propanol. The superior photocatalytic performances are investigated to be the synergistic effect of hollow structures and crystal planes exposed.

Acknowledgements

This work was financially supported by the National Nature Science Foundation of China (21071036 and 21271055) and Province Natural Science Foundation of Heilongjiang Province (ZD201011). We acknowledge the State Key Laboratory of Urban Water Resource and Environment for the help in characterization.

References

[1] A. Kudo, Y. Miseki, Chemical Society Reviews 38 (2009) 253.
[2] R.M. Navarro Yerga, M.C. Álvarez Galván, F. del Valle, J.A. Villoria de la Mano, J.L.G. Fierro, ChemSusChem 2 (2009) 471–485.
[3] X.B. Chen, S.H. Shen, L.J. Guo, S.S. Mao, Chemical Reviews 110 (2010) 6503–6570.
[4] D.L. Zhao, G.D. Sheng, C.L. Chen, X.K. Wang, Applied Catalysis B: Environmental 111 (2012) 303–308.
[5] H.G. Yu, R. Liu, X.F. Wang, P. Wang, J.G. Yu, Applied Catalysis B: Environmental 111 (2012) 326–333.
[6] M. Oshikiri, M. Boero, Journal of Physical Chemistry B 110 (2006) 9188–9194.
[7] H. Fan, D. Wang, L. Wang, H. Li, P. Wang, T. Jiang, T. Xie, Applied Surface Science 257 (2011) 7758–7762.
[8] H. Tong, S. Ouyang, Y. Bi, N. Umezawa, M. Oshikiri, J. Ye, Advanced Materials 24 (2012) 229–251.
[9] J.H. Xu, W.Z. Wang, S.M. Sun, L. Wang, Applied Catalysis B: Environmental 111 (2012) 126–132.
[10] S. Murphy, C. Saurel, A. Morrissey, J. Tobin, M. Oelgemoller, K. Nolan, Applied Catalysis B: Environmental 119 (2012) 156–165.
[11] Z. Yi, J. Ye, N. Kikugawa, T. Kako, S. Ouyang, H. Stuart-Williams, H. Yang, J. Cao, W. Luo, Z. Li, Y. Liu, R.L. Withers, Nature Materials 9 (2010) 559–564.
[12] Y. Bi, S. Ouyang, N. Umezawa, J. Cao, J. Ye, Journal of the American Chemical Society 133 (2011) 6490–6492.
[13] L. Wang, W. Wang, M. Shang, S. Sun, W. Yin, J. Ren, J. Zhou, Journal of Materials Chemistry 20 (2010) 8405.
[14] L. Ye, L. Zan, L. Tian, T. Peng, J. Zhang, Chemical Communications 47 (2011) 6951–6953.
[15] J. Xia, S. Yin, H. Li, H. Xu, Y. Yan, Q. Zhang, Langmuir 27 (2011) 1200–1206.
[16] J. Xia, S. Yin, H. Li, H. Xu, L. Xu, Y. Xu, Dalton Transactions 40 (2011) 5249–5258.
[17] H. Fu, C. Pan, W. Yao, Y. Zhu, Journal of Physical Chemistry B 109 (2005) 22432–22439.
[18] C. Wang, L. Zhu, M. Wei, P. Chen, G. Shan, Water Research 46 (2012) 845–853.
[19] L. Kong, Z. Jiang, T. Xiao, L. Lu, M.O. Jones, P.P. Edwards, Chemical Communications 47 (2011) 5512–5514.
[20] H. Cheng, B. Huang, P. Wang, Z. Wang, Z. Lou, J. Wang, X. Qin, X. Zhang, Y. Dai, Chemical Communications 47 (2011) 7054–7056.
[21] Q.C. Xu, Y.H. Ng, Y. Zhang, J.S. Loo, R. Amal, T.T. Tan, Chemical Communications 47 (2011) 8641–8643.
[22] G. Dai, J. Yu, G. Liu, Journal of Physical Chemistry C 115 (2011) 7339–7346.
[23] A. Fujishima, K. Honda, Nature 238 (1972) 37–38.
[24] M.L. Guan, D.K. Ma, S.W. Hu, Y.J. Chen, S.M. Huang, Inorganic Chemistry 50 (2011) 800–805.
[25] J.Z. Su, L.J. Guo, S. Yoriya, C.A. Grimes, Crystal Growth and Design 10 (2010) 856–861.
[26] D. Wang, H. Jiang, X. Zong, Q. Xu, Y. Ma, G. Li, C. Li, Chemistry- A European Journal 17 (2011) 1275–1282.
[27] L. Zhang, D. Chen, X. Jiao, Journal of Physical Chemistry B 110 (2006) 2668–2673.
[28] G. Xi, J. Ye, Chemical Communications 46 (2010) 1893–1895.
[29] J. Su, L. Guo, N. Bao, C.A. Grimes, Nano Letters 11 (2011) 1928–1933.
[30] A.R. Lim, S.H. Choh, M.S. Jang, Journal of Physics: Condensed Matter 7 (1995) 7309–7323.
[31] X. Zhang, Z. Ai, F. Jia, L. Zhang, X. Fan, Z. Zou, Materials Chemistry and Physics 103 (2007) 162–167.
[32] H. Fan, T. Jiang, H. Li, D. Wang, L. Wang, J. Zhai, D. He, P. Wang, T. Xie, Journal of Physical Chemistry C 116 (2012) 2425–2430.
[33] Q.H. Xiao, Y. Zhu, J. Guo, J.A. Wang, Y.M. Zhang, Chinese Journal of Inorganic Chemistry 27 (2011) 19–24.
[34] Z. Wang, W. Luo, S. Yan, J. Feng, Z. Zhao, Y. Zhu, Z. Li, Z. Zou, CrystEngComm 13 (2011) 2500.
[35] Y. Liu, J. Ma, Z. Liu, C. Dai, Z. Song, Y. Sun, J. Fang, J. Zhao, Ceramics International 36 (2010) 2073–2077.
[36] W.T. Sun, M.Z. Xie, L.Q. Jing, Y.B. Luan, H.G. Fu, Journal of Solid State Chemistry 184 (2011) 3050–3054.
[37] M. Ge, L. Liu, W. Chen, Z. Zhou, CrystEngComm 14 (2012) 1038–1044.
[38] S.S. Dunkle, R.J. Helmich, K.S. Suslick, Journal of Physical Chemistry C 113 (2009) 11980–11983.
[39] M.C. Neves, T. Trindade, Thin Solid Films 406 (2002) 93–97.
[40] J.B. Liu, H. Wang, H.M. Zhang, W.X. Zhang, H. Yan, Chinese Journal of Inorganic Chemistry 23 (2007) 1299–1302.
[41] H.B. Li, G.C. Liu, X.C. Duan, Materials Chemistry and Physics 115 (2009) 9–13.
[42] W. Liu, Y.Q. Yu, L.X. Cao, G. Su, X.Y. Liu, L. Zhang, Y.G. Wang, Journal of Hazardous Materials 181 (2010) 1102–1108.
[43] X.W. Lou, L.A. Archer, Z. Yang, Advanced Materials 20 (2008) 3987–4019.

[44] W.Z. Yin, W.Z. Wang, M. Shang, L. Zhou, S.M. Sun, L. Wang, European Journal of Inorganic Chemistry (2009) 4379–4384.
[45] W. Liu, L.X. Cao, G. Su, H.S. Liu, X.F. Wang, L. Zhang, Ultrasonics Sonochemistry 17 (2010) 669–674.
[46] C.H. Deng, H.M. Hu, W.L. Zhu, C.L. Han, G.Q. Shao, Materials Letters 65 (2011) 575–578.
[47] P. Madhusudan, J. Ran, J. Zhang, J. Yu, G. Liu, Applied Catalysis B: Environmental 110 (2011) 286–295.
[48] X. Zou, B.B. Liu, Q.J. Li, Z.P. Li, B. Liu, W. Wu, Q.A. Zhao, Y.M. Sui, D.M. Li, B. Zou, T.A. Cui, G.T. Zou, H.K. Mao, CrystEngComm 13 (2011) 979–984.
[49] L. Zhou, W.Z. Wang, L. Zhang, H.L. Xu, W. Zhu, Journal of Physical Chemistry C 111 (2007) 13659–13664.
[50] L. Dong, S. Guo, S.Y. Zhu, D.F. Xu, L.L. Zhang, M.X. Huo, X. Yang, Catalysis Communications 16 (2011) 250–254.
[51] M. Long, W.M. Cai, J. Cai, B.X. Zhou, X.Y. Chai, Y.H. Wu, Journal of Physical Chemistry B 110 (2006) 20211–20216.
[52] M. Stylidi, D.I. Kondarides, X.E. Verykios, Applied Catalysis B: Environmental 47 (2004) 189–201.
[53] T.B. Li, G. Chen, C. Zhou, Z.Y. Shen, R.C. Jin, J.X. Sun, Dalton Transactions 40 (2011) 6751–6758.
[54] Y.F. Qiu, L. Wang, C.F. Leung, G.J. Liu, S.H. Yang, T.C. Lau, Applied Catalysis A: General 402 (2011) 23–30.
[55] X.L. Yan, T. Ohno, K. Nishijima, R. Abe, B. Ohtani, Chemical Physics Letters 429 (2006) 606–610.
[56] F. Amano, T. Yasumoto, T. Shibayama, S. Uchida, B. Ohtani, Applied Catalysis B: Environmental 89 (2009) 583–589.
[57] S. Kitano, K. Hashimoto, H. Kominami, Applied Catalysis B: Environmental 101 (2011) 206–211.